Analog VLSI Circuit Implementation of an Adaptive Neuromorphic Olfaction Chip

Thomas Jacob Koickal, Alister Hamilton, Su Lim Tan, *Member, IEEE*, James A. Covington, Julian W. Gardner, *Senior Member, IEEE*, and Tim C. Pearce

***Abstract*—In this paper, we present the analog circuit design and implementation of the components of an adaptive neuromorphic olfaction chip. A chemical sensor array employing carbon black composite sensing materials with integrated signal processing circuitry forms the front end of the chip. The sensor signal processing circuitry includes a dc offset cancellation circuit to ameliorate loss of measurement range associated with chemical sensors. Drawing inspiration from biological olfactory systems, the analog circuits used to process signals from the on-chip odor sensors make use of temporal "spiking" signals to act as carriers of odor information. An on-chip spike time dependent learning circuit is integrated to dynamically adapt weights for odor detection and classification. All the component subsystems implemented on chip have been successfully tested in silicon.**

***Index Terms*—Analog VLSI, electronic nose, machine olfaction, neuromorphic circuits, on-chip learning, spike-timing-dependent plasticity (STDP).**

I. Introduction

THE olfactory pathway is particularly impressive in its ability to detect and identify an extremely wide range of both simple and complex odors with high sensitivity [1]. The sensing capabilities of a dog's nose, for instance, are well beyond that achievable by any existing technological chemical sensing equivalent, both in terms of its combined specificity and its sensitivity to individual compounds. Achieving such detection performance requires the complex orchestration of a whole series of events, beginning with the rapid and efficient transport of ligands to the sensing site, simultaneous detection of a wide diversity of ligands, through to the formation and subsequent decoding of the neural signal representations of odors in the nervous system.

Only recently have technological advances in chemosensors, MEMS, silicon integration [2]–[4] and the basic understanding of the neuroscience of olfaction [5] made it possible to consider implementing a single, fully integrated neuromorphic olfaction chip. Here we describe the implementation and test results from each of the functional subcomponents of such a system. Our approach is in contrast to previous chemical detection systems based upon the olfactory pathway, which have addressed: sensing [6], signal processing [7]–[9], and neuromorphic simulation models [10]–[12], separately. Traditional machine olfaction or electronic nose systems typically use conventional software based pattern recognition techniques or multirate analysis using data from a series of discrete chemical sensors rather than modeling biology directly [3]. While artificial neural networks such as the multilayer perceptron have been used for pattern recognition in electronic nose systems [13], [14], spiking neural models are more biologically plausible [15].

Biological [16] and theoretical [17], [18] studies indicate that temporal spike time based coding can be used to implement powerful information processing systems [19]. Experimental studies have shown that the precise timing of spikes generated by neurons can be critical for the direction and magnitude of synaptic weight changes; a phenomenon known as spike-timing-dependent plasticity (STDP) [18], [20]–[22]. Spike timing dependent learning rules can be used to learn temporal delays with high precision and have been used to model auditory processing in the barn owl [17] and vision systems [23].

This work brings together integrated sensor technology and systems using spike time based neuromorphic models to implement an olfactory system in analog VLSI. The use of analog VLSI allows for low power operation, low cost and area efficient hardware realizations. More importantly, a neuromorphic implementation promises to offer a solution to the many attendant signal processing issues related to complex odor detection, in particular odor segmentation and odor object identification in varying chemical environments which have yet to be solved with classical approaches [10], [11]. Thus, such a system has potential portable sensing applications where there is a requirement for discrimination against a wide variation in background odor signals, for example in medical diagnostics.

In this paper, we present the analog VLSI design, implementation and test results of the component circuits for an adaptive neuromorphic olfaction chip developed over a number of chip implementation cycles. An analog VLSI device with on-chip chemosensor array, on-chip sensor interface circuitry and on-chip adaptive neuromorphic olfactory model has been fabricated in a single chip using these functional circuit components. The block diagram of this fabricated chip is shown in Fig. 1. The architecture of the chip implements a slice of the olfactory network such that a scalable olfactory system can be

Manuscript received January 31, 2006; revised September 11, 2006. This work was supported by the Engineering and Physical Sciences Research Council (EPSRC), U.K., under Grant GR/R37982/01 to University of Edinburgh, Grant GR/R37975/01 to University of Warwick, and Grant GR/R37968/01 to University of Leicester. This paper was recommended by Guest Editor D. Wilson.

T. J. Koickal and A. Hamilton are with the School of Engineering and Electronics, University of Edinburgh, Edinburgh EH9 3JL, U.K (e-mail: thomas.koickal@ee.ed.ac.uk, alister.hamilton@ee.ed.ac.uk).

S. L. Tan, J. A. Covington, and J. W. Gardner are with the Sensors Research Laboratory, University of Warwick, Warwick CV4 7AL, U.K (e-mail: j.w.gardner@warwick.ac.uk).

T. C. Pearce is with the Department of Engineering, University of Leicester, Leicester LE1 7RH, U.K (e-mail: tcp1@leicester.ac.uk).

Digital Object Identifier 10.1109/TCSI.2006.888677

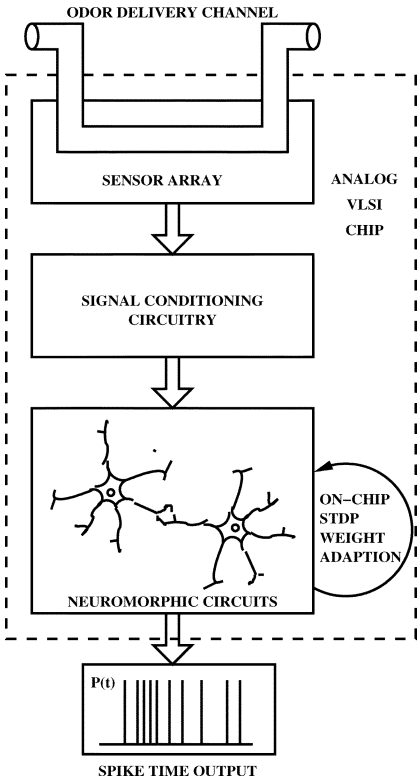

Fig. 1. Block diagram of an analog VLSI implementation of an olfactory pathway with STDP on-chip learning.

constructed by interconnecting multiple chips. The olfactory sensors implemented on chip comprise a resistive chemosensor array employing carbon black (CB) composite sensing materials with integrated signal processing circuitry. The sensor interface circuitry includes a dc cancellation circuit to ameliorate loss of measurement range associated with chemical sensors. A spiking neural architecture forms the signal processing stage of the olfactory bulb model. An on-chip spike-time-dependent learning circuit is integrated to dynamically adapt weights for odor detection and classification. Implementation of on-chip learning is crucial for the design of an integrated odor sensing system. This not only emulates the plasticity function found in biological neural systems but also provides a means to compensate for analog imperfections in the physical implementation as well as changes in the environmental conditions in which the device must operate. All the component circuits implemented on the fabricated chip have been successfully tested in silicon, as we report here.

II. Description of Olfactory Pathway Model

A. Biological Olfactory Model

A large number of olfactory receptor neurons (ORNs) constitute the front-end of the mammalian olfactory system which are responsible for detecting airborne molecules. Cilia of ORNs protrude into the olfactory mucosa, where they come in contact with molecules that are transported by the nasal airflow. On the surface of the cilia, odorant receptors (ORs) bind odorant molecules with a broadly tuned affinity. When an OR binds with an odorant molecule, it triggers in its ORN a bio-chemical cascade that eventually causes the membrane potential of the ORN to change, potentially leading to the generation of spikes. Each ORN only expresses one type of OR, while each type of receptor is usually expressed by a large number of ORNs; for example, in mice around 1 000 types of ORs are expressed by millions of ORNs [5].

ORNs project their axons to the olfactory bulb, terminating at spherical neuropil called glomeruli where they mainly synapse onto the dendrites of mitral and tufted (M/T) cells, which act as a principal neurons (PNs). Experimental data indicates that each glomerulus receives axons from only ORNs expressing the same type of OR [24], while a single PN sends its aprical dendrite to a single glomerulus [25]. Inhibitory neurons of the olfactory bulb (granule cells) make reciprocal contacts with many PNs, forming together a complex network constituting the first stage of olfactory information processing. The output of PNs are relayed to higher brain area for further processing.

B. Neuromorphic Olfactory Model

Drawing inspiration from the architecture of the olfactory pathway presented in the previous section, a neuromorphic architecture, shown in Fig. 2, with chemosensors has been implemented. The neuromorphic network receives sensory signals from an array of chemosensors which transform the molecular chemical information of an odorant into electrical signals suitable for processing in analog circuitry. The chemosensor array consist of different sensor types tuned to respond to different chemical compounds. Such a heterogeneous array has the potential to increase the selectivity in the olfactory pattern recognition task while mimicking the function of the mammalian olfactory system [5], [26].

Chemosensory signals are transformed into spike trains by ORN models. These spike trains directly drive synaptic currents which are then summed for the purposes of signal enhancement and stability in the face of individual sensor drift. This summed signal provides the excitatory drive to PNs, which in turn provide the main output of the system. Lateral inhibitory neurons are used to both sharpen the output characteristics of the system compared to the original chemosensory input pattern, but also to implement attractor dynamics in the system which make it capable of learning and completing particular input patterns.

Because the signals from sensors of the same type are fed forward through neural elements to one and one only PN, the network forms a distinct modular structure, reminiscent of the glomerular organization of the biological olfactory bulb model [5]. Furthermore, receptor neurons and PNs shown in Fig. 2 represent the biological model elements of ORNs and M/T cells, respectively.

C. Model Dynamics

The soma of each neuron element is modeled as a leaky integrate and fire (IF) unit. Below a threshold $V_{\rm th}$ the dynamics of the membrane potential $V_m(t)$ of the IF neuron is defined by

$$\frac{dV_m(t)}{dt} = -\frac{V_m(t) - V_{\rm rest}}{R_m C_m} + \frac{I(t)}{C_m} \tag{1}$$

where t is time, R_m and C_m are, respectively, the membrane resistance and capacitance, and $I(t)$ is the total input current to the

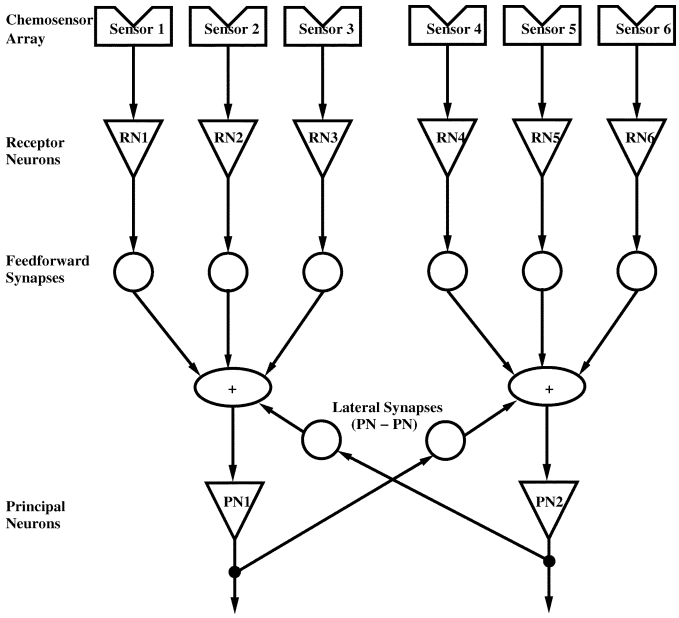

Fig. 2. Slice of the neuromorphic olfactory model. RN1 to RN3 are fed from sensors of the same type, similarly for RN4 to RN6. Here, RNs correspond to biological ORNs, PNs to M/T cells, and lateral synapses to granule cells. Weight adaption at all synapses using STDP.

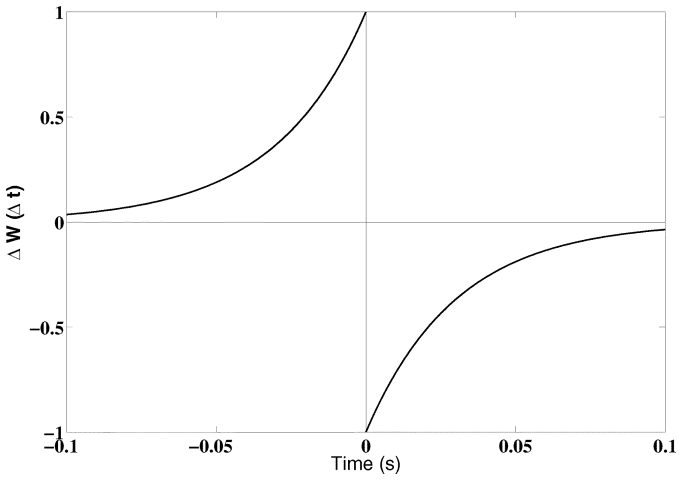

Fig. 3. STDP learning window function implemented on chip. The change in weight with respect to the time difference between pre- and post-synaptic neuron firing [18].

neuron. $V_{\rm rest}$ is the membrane resting potential. If the potential $V_m(t)$ reaches the threshold value $V_{\rm th}$ it is immediately reset to the after hyperpolarization value $V_{\rm ahp}$ and a spike is produced as neuron output. The emission of any spike is followed by a refractory time period, during which the neuron cannot fire but will continue to integrate the input currents.

When a spike reaches a synapse, it induces a dendritic current that is fed into the postsynaptic neuron which decays exponentially with a characteristic time constant, starting from a peak value determined by the synaptic weight. The sign of the current is formally included into the synaptic weight, positive or negative according to whether the interaction is, respectively, excitatory or inhibitory. If $t = 0$ is the instant at which the spike from a presynaptic neuron A reaches the synapse of A onto postsynaptic neuron B, the current evoked onto B by this single event is given by

$$i_{BA}(t) = \Theta(t) w_{BA} \exp^{-t/\tau_d} \tag{2}$$

where $\Theta(t)$ is the Heaviside function, w_{BA} is the synaptic weight, and τ_d is the synaptic time constant. The total current induced by several presynaptic spikes by neuron A onto postsynaptic neuron B is given by

$$I_{BA}(t) = \sum_n i_{BA}(t - t_n) \tag{3}$$

where n indexes the spikes that are emitted by neuron A and reach the synapse at times t_n. If a neuron receives the outputs of several synapses, the respective contributions to the total postsynaptic current sum linearly. The total postsynaptic current constitutes the term $I(t)$ in (1), from which the membrane potential of the respective neuron is derived.

D. Weight Adaptation

In the neuromorphic model implemented, the network learns odorant features by modifying weights of all synapses according to a temporally asymmetric spike-time-dependent Hebbian learning rule [18], [22]. In STDP, if a presynaptic spike arrives at the synaptic terminal before a postsynaptic spike is emitted and within a critical time window, the synaptic efficacy is increased. Conversely, if the postsynaptic spike is emitted prior to the arrival of the presynaptic spike, the synaptic efficacy is decreased. The neuromorphic olfactory model (Fig. 2) implements an STDP based learning window function shown in Fig. 3 for synaptic weight adaption. The learning window function for weight adaption is defined as follows:

$$\Delta W(\Delta t) = \begin{cases} A_+ \exp\left(\frac{(-\Delta t)}{t_{ln+}}\right), & \text{if } \Delta t > 0 \\ -A_- \exp\left(\frac{(\Delta t)}{t_{ln-}}\right), & \text{if } \Delta t \leq 0 \end{cases} \tag{4}$$

where $\Delta t = t_{\rm post} - t_{\rm pre}$, is the time delay between postsynaptic neuron firing $t_{\rm post}$ and presynaptic firing $t_{\rm pre}$. In (4), ΔW determines the synaptic weight change for a time delay Δt. The learning window has two phases: a positive phase of synaptic potentiation for positive Δt and a negative phase of synaptic depression for negative Δt [see (4)]. The dynamics of the positive phase are generated by a presynaptic spike arrival and dynamics of the negative phase are generated by a postsynaptic spike arrival. The time constant parameters t_{ln+} and t_{ln-} determine the range of Δt over which synaptic weight adaption occur.

The neural signals of the proposed model encode odor information in temporal sequences. An STDP based weight adaptation introduces predictive coding to classical Hebbian learning rule [18]. If a feature in the odor input generates presynaptic spike pattern that can reliably predict the occurrence of a postsynaptic spike and seldom comes after a postsynaptic spike, the synapses related to that odor feature are strengthened giving that feature more control over the firing of the postsynaptic neuron.

The predictive occurrence of spike timing patterns could possibly lead to an odor detection and encoding mechanism in the olfactory pathway.

III. Analog Circuit Design of Neuromorphic Olfaction Chip

A. Chemosensor Array

The input to the olfactory bulb model is provided by a chemosensor array fabricated using Austria Micro Systems (AMS) 0.6-μm CMOS process with post processing to deposit odor sensitive material. In this case a chemoresistive sensor array has been formed where the sensor responses are measured as a change in resistance of a chemically sensitive film. The coatings used here are CB polymer materials, whose response depends upon the target odor used for the olfaction pattern recognition task. These materials operate by combining an insulating rubber with carbon nanospheres that endow electrical conduction to the resultant mix. Individual chemoresistive sensors are created by depositing CB polymer material between two sensor electrodes.

The resistance of the sensor is directly proportional to the aspect ratio (length over width) of the inter-electrode gap and the carbon doping of the polymer. Exposure to an odor causes specific chemical components to diffuse into the polymer resulting in expansion (swelling) thus increasing the gap between the carbon spheres and thereby increasing the resistance of the polymer composite film [27]. By altering the rubber, it is possible to vary the sensitivity of the sensor to different chemical components within the odor.

In our implementation, each sensor cell contains a programmable current source, a sensor, and a baseline cancellation circuit. Other chemical sensing arrays [28] with higher density employ a multiplexing mechanism to provide access to individual sensors without any complex circuitry. However, the challenge here is to create a sensor array with individual direct output so that the continuous sensor responses can be interfaced to neuronal circuits without any multiplexing. Moreover, as each sensor has a dedicated set of circuitry, each of them may be biased and amplified optimally.

B. Signal Conditioning Circuitry

Although a heterogeneous array of resistive chemical sensors can improve the selectivity performance for an olfactory pattern recognition task, the design of a suitable signal conditioning circuit for the array poses considerable challenges. An undesirable characteristic associated with a heterogeneous chemosensor array is the large variation in baseline dc signals among the different sensors types in the array [29]. The large variation of baseline signals for a chemosensor array are caused by: 1) the poisoning effect during post-processing of the chemosensor array; and 2) different optimal operating current specifications for different sensor types. The large variation in baseline dc signals among the sensors may result in saturation of the subsequent signal conditioning amplifier stages thereby leading to loss of measurement range which cannot be recovered [30], [31].

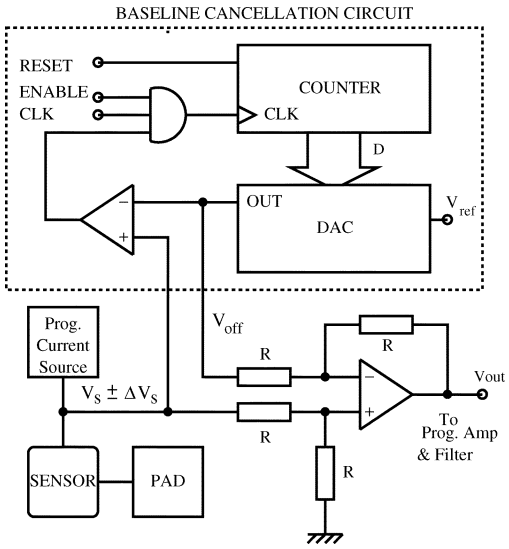

Fig. 4. Simplified schematic of the sensor interface circuit. Each sensor is driven a programmable current source. The baseline cancellation circuit and the difference amplifier cancel the baseline variation of the sensor. The output of the sensor interface is a continuous time analog signal.

A common approach to dc signal cancellation is to use a reference chemical sensor driven by the same operating conditions to derive the common dc operating point. However, such an approach is not appropriate here because the primary cause of baseline variation is a poisoning effect during postprocessing. The poisoning effect causes the reference chemical sensor to have different dc operating conditions to the sensor whose dc signal we are trying to cancel, hence this approach is not appropriate here. A schematic of the sensor interface electronics for canceling the baseline dc signals is shown in Fig. 4. Prior to measurement, there is a setup phase during which the baseline signals of all sensors in the array are digitally stored using a simple counting analog to digital converter. The output from the internal digital to analog converter provides the initial analog offset signal which is then canceled using a difference amplifier. The output sensor interface circuit is maintained in analog continuous time domain and feeds into the subsequent neuromorphic circuit stage implemented on chip.

C. Synapse Circuit

The synapse circuit shown in Fig. 5 consists of a weight dynamics block and a synapse dynamics block. These are formed by two balanced OTA structures (M1-M9) and (M16-M24). The outputs of these OTA structures are fed back to their inverting inputs and they behave as resistors. The weight voltage $V_{\rm wt}$ stored on capacitor $C_{\rm wt}$ during on-chip learning forms the input to the weight dynamics block. The input to the synapse is a presynaptic spike $V_{\rm spike}$ whose leading edge switches the transmission gate switch (M11-M12) ON and the capacitor $C_{\rm syn}$ starts to charge toward $V_{\rm wt}$. The OTA (M1-M9) is designed for small output currents ($i_{\rm wt} < 500$ pA) and the neuronal spike width is narrow ($\Delta T < 100$ μs). Therefore, the injection of a weight current $i_{\rm wt}$ results in only a small voltage change at the synapse capacitor $C_{\rm syn}$. The trailing edge of the presynaptic neuronal spike switches the transmission gate (M11-M12) OFF and $C_{\rm syn}$ begins

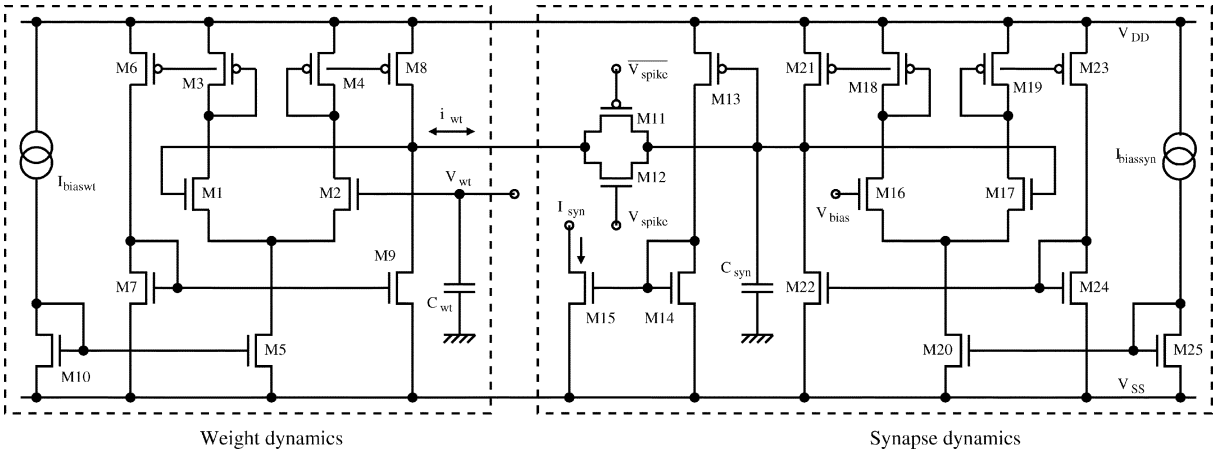

Fig. 5. Synapse circuit based on two OTA-C structures. The weight is stored on C_{wt}. The presynaptic spike signal V_{spike} induces charging or discharging of C_{syn}. The synapse output is the current i_{syn}.

to discharge exponentially toward V_{bias} of OTA (M16-M24). A subsequent spike will cause a further injection (or removal) of current and a further incremental (or decremental) change in the voltage on the synapse capacitor C_{syn}. The exponential voltage response controls the gate of a transistor M13 biased in the linear region to form an exponential output current i_{syn}. The synaptic output currents from various synapses are summed at the neuronal input.

The design of analog circuits with large time constants is critical for the implementation of a neuromorphic olfaction chip. This is because the chemical sensors have large time constants, typically in the order of 100 ms or more [6], which translates into large time constant requirements for the neuron and synapse models. In the design implemented on chip, large time constants are achieved by reducing the transconductance of the OTA stage thereby alleviating the need for implementing large area capacitors [32]. The transconductance reduction in the OTA stage is achieved by using large current mirror ratios. Noting the transconductance of an OTA is proportional to the ratio of the size of the output current mirrors (M22/M24) a multiplication of time constant by K can be obtained. The advantage of this approach is that subthreshold currents exist in the output stage transistors (M21, M22) while all other transistors of the synapse dynamics circuit operate in the strong inversion region. The offset voltage of this OTA resistor is thus primarily determined by the leakage currents in the output node. The larger biasing currents in the OTA input transistors result in a larger linear range with reduced offset mismatching in layout. A programmable time constant can be achieved by using different dimension ratios at the output current mirror branch.

Several synaptic circuits have been reported in the literature [33]–[38]. The synaptic circuit implemented in [34] has an exponentially decaying synaptic current which always resets to a fixed current value during each spike event. This circuit is not suitable for summation of multiple synaptic events as modeled here. The synaptic circuits implemented in [35] and its variations [36]–[38] use simple and compact circuits to implement synaptic currents. However, these circuits have limited control on varying the synaptic parameters independently. The circuit in [39] implements summation of exponentially decaying synaptic currents for multiple spike events. This circuit needs separate outputs for generating inhibitory and excitatory synapses; an inhibitory synaptic output requires an nMOS output transistor while a separate pMOS output transistor is required to output an excitatory response. In the implementation presented here, the synapse circuit can produce both excitatory and inhibitory responses at the same output depending on the sign of the weight voltage. In general, the synaptic circuits reported in the literature have time constants in the range of 10–50 ms, which is typically an order of magnitude lower that required in this olfactory system implementation.

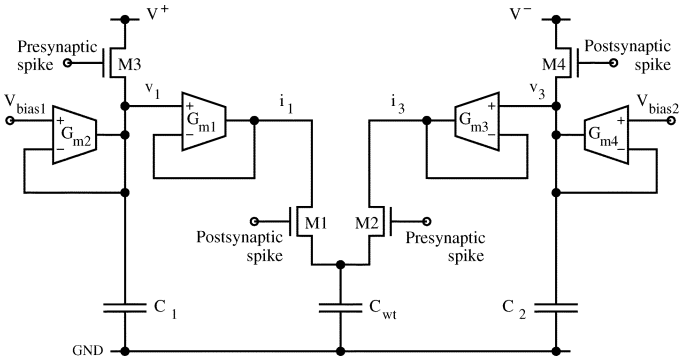

Fig. 6. Simplified schematic of the STDP learning circuit formed by two symmetrical circuit blocks to implement the positive and negative phases of the learning function.

D. On-Chip STDP Learning Circuit

In STDP learning, the relative time interval between the postsynaptic neuron firing and the presynaptic spike occurrence determines the weight change at the weight storage capacitor C_{wt}. Each synapse has an STDP based on-chip learning circuit associated with the capacitor C_{wt}. The component C_{wt} in Fig. 5 is the same as the component C_{wt} in Fig. 6.

The circuit uses two identical circuit blocks to define the positive phase and the negative phase of the learning window function. The four OTA circuits in Fig. 6 use the same low transconductance design as outlined in Section III-C. The weight adap-

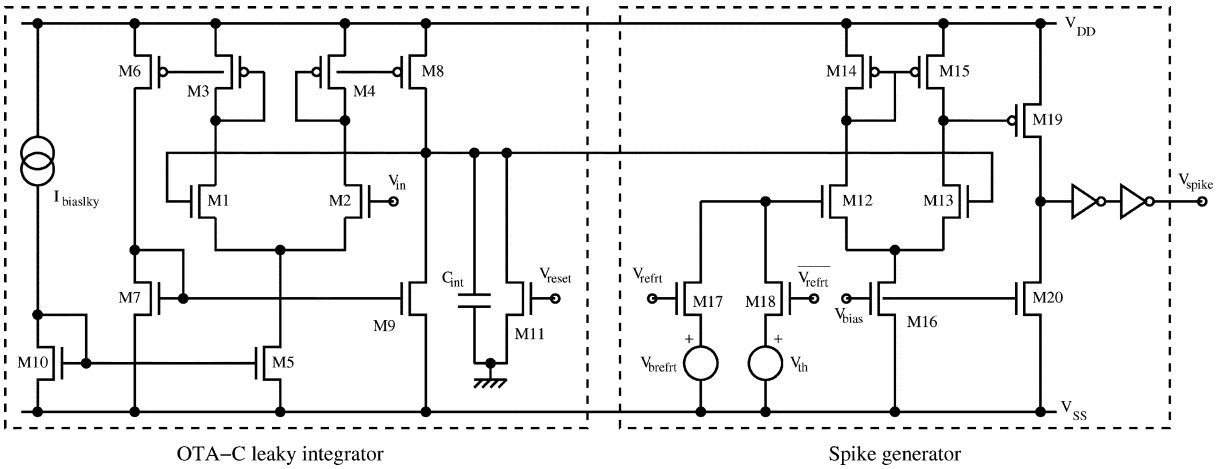

Fig. 7. Neuron circuit based on an OTA-C leaky integrator. The membrane potential is represented by the voltage on $C_{\rm int}$. Transistors M12-M20 implement the spike generation circuitry. The refractory period timer circuit is also based upon an OTA-C structure (not shown) and generates $V_{\rm refrt}$.

tion during the positive phase of the learning window function operates as follows. A presynaptic spike occurrence turns transistor M3 ON charging the capacitor C_1 to V_+. The trailing edge of the presynaptic spike switches the transistor M3 OFF and the voltage v_1 at the capacitor C_1 decays exponentially to a resting potential $V_{1\,\rm min}$. The time constant of the exponential response during this phase is given by the ratio C_1/G_{m2}. On the arrival of a postsynaptic spike, the transistor M1 is switched ON and the weight voltage $V_{\rm wt1}$ at the capacitor $C_{\rm wt}$ begins to charge toward V_1, where V_1 is the voltage across C_1 at the instant of postsynaptic spike arrival. Due to the small output currents ($i_1 < 500$ pA) from transconductor G_{m1} and the narrow neuronal spike width ($\Delta T < 100\ \mu$s), the capacitor weight voltage $V_{\rm wt}$ charges to a fraction of the final voltage V_1. This results in an incremental change in the weight voltage $V_{\rm wt}$ at each post synaptic spike occurrence.

The resulting change in weight voltage is $\Delta V_{\rm wt} = (V_1 - V_{\rm wt1})G_{m1}\Delta T/C_{\rm wt}$. Thus, the incremental weight change, $\Delta V_{\rm wt}$ is an exponential function of the time difference between the postsynaptic spike arrival and presynaptic spike arrival. For a constant V_1, the incremental weight change $\Delta V_{\rm wt}$ at each postsynaptic spike become smaller as the capacitor incrementally charges toward its peak voltage $V_{\rm wt\,max}$. The change in weight voltage $\Delta V_{\rm wt} \geq 0$, if $V_{\rm wt\,max} \leq V_{1\,\rm min}$; the resting voltage $V_{1\,\rm min}$ is defined by the externally controllable bias voltage $V_{\rm bias1}$.

Similarly, during the negative phase, a postsynaptic spike triggers an exponential response at capacitor C_2 and a following presynaptic spike decrements the weight at $C_{\rm wt}$. The weight voltage at $C_{\rm wt}$ is strengthened, if the presynaptic spike precedes the postsynaptic arrival and weakened if the presynaptic spike follows the postsynaptic occurrence. The STDP learning we have implemented is a dynamic learning mechanism and weight voltages stored on $C_{\rm wt}$ will decay if not refreshed. Long term weight storage can be performed by storing the weight voltage stored on $C_{\rm wt}$ in a non-volatile memory.

STDP based on-chip learning circuits have been reported in literature [40], [41]. The STDP learning circuit in [40] implements a learning window function which is a linear function of the time difference between the postsynaptic spike and presynaptic spike arrival. This is in contrast to the exponential learning window function (see Fig. 3) implemented on this chip which has a closer resemblance to the experimental results observed in biology [20]. Furthermore, the on-chip STDP circuit is implemented in full analog unlike the circuit implementation reported in [41] that included digital circuits.

E. Neuron Circuit

A circuit schematic of the integrate and fire neuron is shown in Fig. 7. The leaky integrator dynamics ((1)) are implemented using an OTA-C circuit. Transistors M1-M7 form an OTA and $C_{\rm int}$ is the integrating capacitor. A two stage comparator circuit compares the output of the leaky integrator against a threshold $V_{\rm th}$. The control signals $V_{\rm reset}$ and $V_{\rm refrt}$ are the outputs of the reset timer and refractory period timer circuits respectively which are both implemented using comparators and OTA-C delay circuits (not shown).

Initially the $V_{\rm reset}$ and $V_{\rm refrt}$ signals are at a low state. The comparator output $V_{\rm spike}$ goes high when the leaky integrator response is above a threshold $V_{\rm th}$. The leading edge of the neuron spike activates the reset and refractory period timers circuits. The reset timer output $V_{\rm reset}$ goes high after a finite time interval which in turn resets the integrating capacitor $C_{\rm int}$ causing the neuron output to go low. The trailing edge of $V_{\rm spike}$ triggers the refractory timer $V_{\rm refrt}$ to a high state. The control signal $V_{\rm refrt}$ switches the comparator threshold $V_{\rm th}$ to a large voltage $V_{\rm brefrt}$ thereby inhibiting the neuron from firing. However, the leaky integrator continues to integrate during the refractory period. The time delay of the reset timer and refractory period circuit timer determines the pulsewidth of the neuron spike and the refractory period, respectively.

IV. Chip Results

A. Chip Details

An adaptive neuromorphic olfaction device consisting of on-chip chemosensor array, on-chip sensor interface circuitry and neuromorphic olfactory circuits with on-chip STDP

learning has been fabricated on a single chip using AMS 0.6-μm CMOS technology. The architecture of the chip implements a slice of the network in Fig. 2 such that a scalable olfactory system can be constructed by interconnecting multiple chips. The sensors in the chip are separated by a distance of 1.2 mm. Each sensor cell has an associated sensor interface circuit for dc cancellation, amplification and filtering. The outputs of sensor interface circuits feed to the inputs of the neuromorphic circuits. The die area of the chip is 50 mm^2 with a core circuit area of 6.5 mm^2, i.e., the chip is pad limited.

The circuit building blocks of the adaptive neuromorphic olfaction chip have been developed in three stages. In the first stage, a sensor array chip of 10 mm $\times$ 5 mm size has been fabricated and tested to characterize the functionality of both sensors and sensor interface circuitry. The sensor array chip consisted of 70 resistive sensors with the associated programmable sensor interface circuitry. The sensor response and performance of the interface circuitry were characterized by delivering target vapors of ethanol and toluene in air. In the second stage, a neuromorphic array chip was fabricated and tested. The chip contained 3 spiking neural network arrays with each array having 3 receptor neurons, 27 synapses and 1 PN. The purpose of this chip was to test the circuit blocks implementing neuromorphic systems. However, the learning in this chip was performed off-chip. In the third and final stage, an adaptive neuromorphic olfaction chip is implemented by integrating the sensor array and neuromorphic circuits together with added on-chip weight adaptation. All the chips were fabricated in AMS 0.6-μm CMOS technology. In this section, we report test results of circuit building blocks developed during the course of the three developmental stages of the adaptive neuromorphic olfaction chip.

B. Post-Processing On-Chip Chemical Sensors

The implementation of the resistive sensor provides two metal pads (60 μm$\times$ 60 μm) separated by a 65 μm gap between which a CB polymer film is deposited. Although a standard CMOS process provides numerous advantages for smart sensor array fabrication, there is an issue with the use of aluminum as the electrode material. Due to the formation of aluminum oxide on the electrodes of the sensor, this has to be gold plated to ensure a stable contact between the sensing material and the aluminum. In this instance, a heat embossing technique using a wire bonder is employed. This technique requires each electrode to be manually coated with several passes using a heated microtip. The result of this gold deposition is less precise with uneven surfaces. However, this does not affect the performance of the circuit.

The five CB polymers used to create the sensing materials are given in Table I. The polymers are either in powder form or small crystals while the CB contains nanospheres with diameter of typically 50–80 nm. The polymer is firstly dissolved in their respective solvent overnight with the aid of a magnetic stirrer at an elevated temperature (50°C). Next, CU is added and the mixture is sonicated for 10 min using a flask shaker. The mixture is then ready for deposition onto the sensors using an airbrush controlled microspraying system. The airbrush is held 10–15 cm away from the micromask (300 μm in diameter) and several passes are sprayed depending on the desired thickness (or resistance). This gives a circular coating typically 350 μm in diameter. The electrical resistance of the deposited polymer sensors can be controlled through the deposition process to a value of about 10 to 200 kΩ with a typical film thickness of about 20 μm ($\pm 50\%$). High resistance variations were observed due to the sensors being deposited in banks (sensors with the same polymer are deposited simultaneously). Finally, the sensor arrays go through a temperature post-treatment at 40°C for 24 h to stabilize the resistance prior to use.

TABLE I
POLYMER MATERIALS USED

No.	Polymer material	Carbon black	Solvent
1	Poly Stylene-cobutadiene (PSB), 0.7g	0.175g	Toluene, 20 ml
2	Poly Ethyl-co-vinyl acetate (PEVA), 1.2g	0.3g,	Toluene, 20 ml
3	Poly Ethylene glycol (PEG), 1.2g	0.3g	Ethanol, 20 ml
4	Poly Caprolactone (PCL), 1.2g	0.3g	Toluene, 20 ml
5	Poly 4-vinyl phenol (PVPH), 1.2g	0.3g	Ethanol, 20 ml

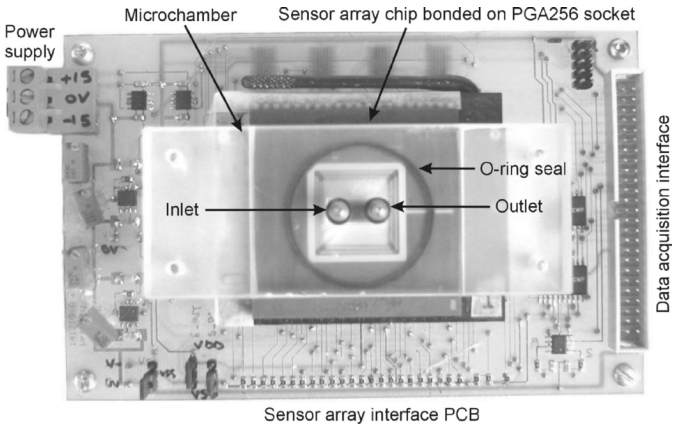

Fig. 8. Experimental setup for odor analysis. The olfaction chip with the chemosensor array has a microchamber mounted on top. Odors are fed to the sensors via the inlet to the microchamber. Sensors on chip are coated with CB polymers.

C. Measured Sensor Response

Fig. 8 shows the experimental setup of the odor analysis system used to characterize the chemosensor array. The odor is delivered through a microchannel placed on top of the fabricated chip. The sensor output (V_s in Fig. 4) can be individually routed to the output of the sensor chip (direct mode) or connected to the baseline cancellation circuit for baseline removal and amplification (interface mode). This facility allows both the sensor and the baseline circuit to be characterized separately. In the direct mode of operation, the baseline cancellation circuit is bypassed and each sensor is connected to a programmable current drive circuit that is cascaded to a buffer op-amp.

The smart sensor cell (incorporating the baseline cancellation circuit in interface mode) was initially characterized for the stability of its constant current drive circuit. Fig. 9(a) shows the change in output voltage across a fixed resistor (used for characterizing the programmable current drive to ensure that the noise fluctuation is due to the current drive and not that of the sensor)

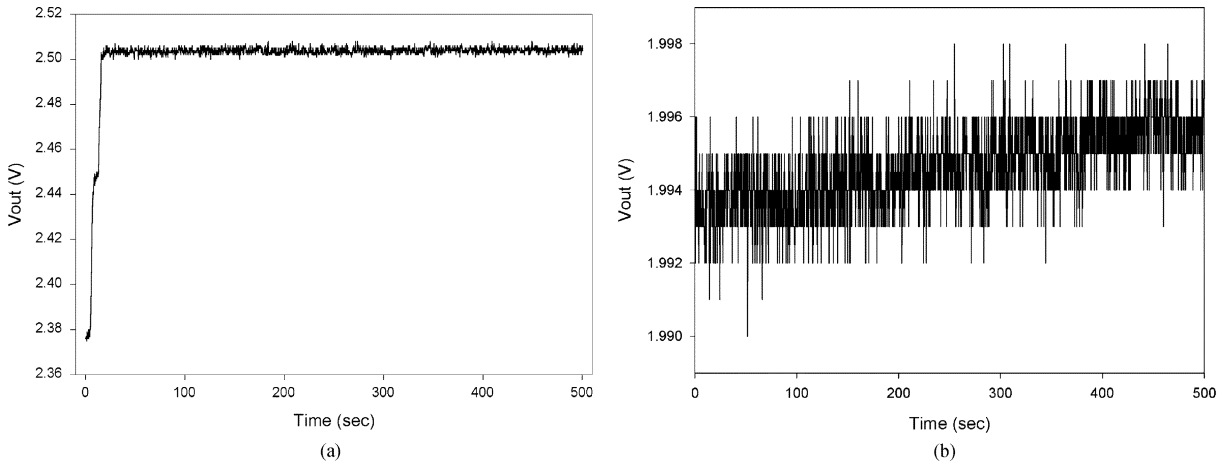

Fig. 9. Driving current and sensor response stability. (a) Constant driving current stability across a fixed resistor. (b) Polymer-composite sensor stability.

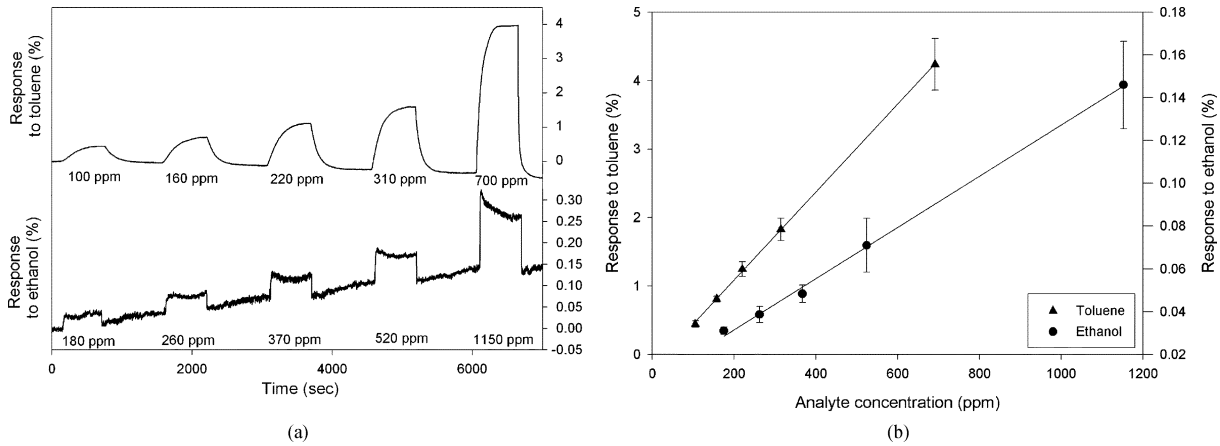

Fig. 10. Sensor response magnitude characterization. (a) Responses of PCB sensor to five different concentrations of ethanol and toluene vapor in air. (b) Static sensor output, fitted with a linear model.

when the current setting was programmed. After a settling period, the noise is found to be within 2 mV. Next, a polymer-composite sensor is coupled to characterize the stability of the sensor output prior to exposure to any analyte. Fig. 9(b) shows the sensor is very stable with noise of within 5 mV.

In the following test, the effect of concentration variation is studied. Here, a Poly Stylene-cobutadiene (PSB) coated sensor, see Table I, has been exposed to five different concentrations of ethanol (180, 260, 370, 520, and 1150 ppm (parts per million)) vapor and toluene (100, 160, 220, 310, and 700 ppm) vapor in air at a constant temperature of 30°C and humidity (20% R.H.) as shown in Fig. 10(a). The response is defined as the percentage change ($\Delta R/R$) in sensor resistance. From these results, the static effect of toluene and ethanol vapor in air to a PSB sensor are plotted as shown in Fig. 10(b). The sensitivity to ethanol vapor is about 0.00012%/ppm and 0.00644%/ppm to toluene vapor. Other types of sensors on chip show similar linear model across the same range of ethanol and toluene vapor concentrations tested here. The drift over time exhibited in Fig. 10(a) is attributed to result of an increase in the environmental (laboratory) temperature.

To further investigate the response characteristics of the sensor array, ethanol and toluene vapor in air are tested at a flow rate of 25 ml/min and pulsewidth of 5 s at room temperature (25°C $\pm$ 2°C, 40% $\pm$ 5% R.H.). The responses of five individual sensors of different sensing material are shown in Fig. 11. Fig. 11(a) shows the responses of five sensors responding to ethanol vapor in air while Fig. 11(b) shows the responses of five sensors responding to toluene vapor in air. The response magnitudes and profiles are unique to each analyte. Transient sensor information is extracted at the neuromorphic circuit stage to aid the discrimination and classification of the input odour as discussed in Section V. The response of the olfactory network is not only sensitive to the pattern of activation across the chemosensor arrays but also to their dynamics. Thus, complex odors eliciting different spatiotemporal patterns may potentially be classified independently.

D. Performance of Sensor Interface Circuitry

The sensors are driven by current sources with programmable output currents of 1, 10, and 100 μA. There are two reasons for providing programmable driving currents over a wide range. Firstly, to accommodate significant variation in sensor baseline resistance as a result of manual deposition process. Secondly, the variation in sensor response due to the selectivity of different sensing materials with target analytes can be adjusted to limit its voltage swing. In the former case, for a sensor resistance of 200 kΩ, the three driving current selections (1, 10, 100 μA) will

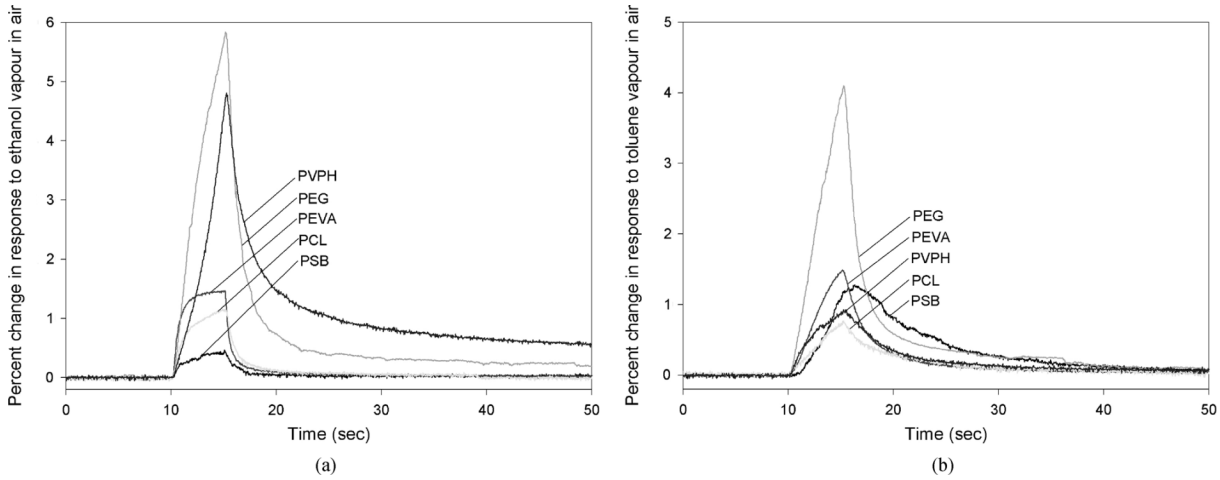

Fig. 11. PSB, PEVA, PEG, PCL, and PVPH sensor response to ethanol and toluene vapor in air. (a) Typical sensor response to ethanol vapor in air. (b) Typical sensor response to toluene vapor in air.

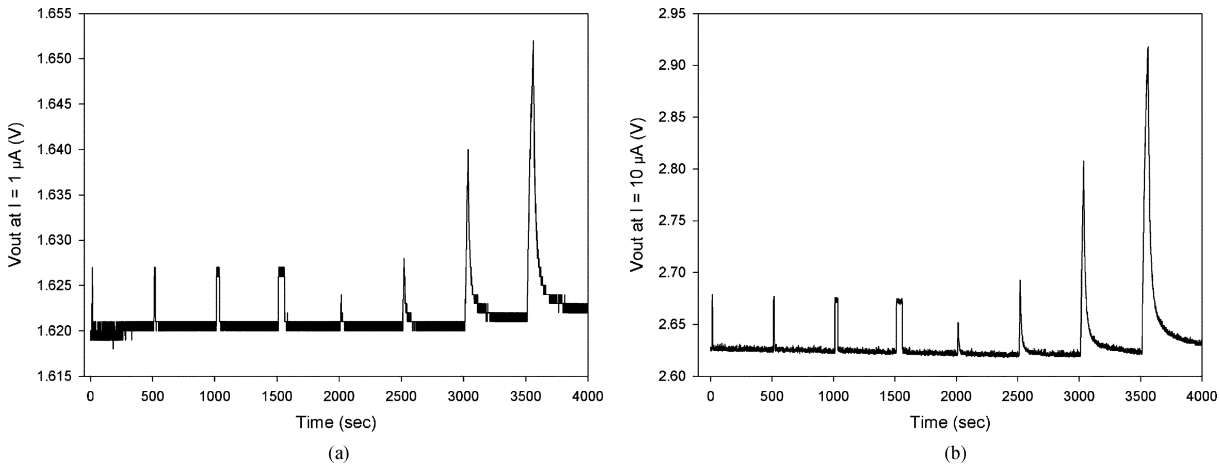

Fig. 12. Effect of varying drive current on sensor response to simple analytes. (a) PEVA sensor response to ethanol and toluene vapor at $I = 1\ \mu$A (offset $= 1.35$ V). (b) PEVA sensor response to ethanol and toluene vapor at $I = 10\ \mu$A (offset $= 0$ V).

ideally produce an output voltage of 200 mV, 2 V, or 20 V. Due to the reduced operating range (5 V) for the CMOS process of the buffer op-amp, the best operating current selection should be $I = 10\ \mu$A to allow the baseline to be in the middle of the operating range ($+2.5$ V, so as to allow maximum positive and negative voltage variations) of the op-amp.

In the latter scenario, the current drive selection is altered to boost the signal level of the response magnitude. Fig. 12(a) shows the response of a Poly Ethyl-co-vinyl acetate (PEVA) coated sensor responding to various pulses of ethanol and toluene vapor in air at $I = 1\ \mu$A (offset voltage $= 1.35$ V) and Fig. 12(b) at $I = 10\ \mu$A (offset voltage $= 0$ V). The response magnitude in Fig. 12(a) is only 30 mV while in Fig. 12(b), the response magnitude is 300 mV, an increase of ten times. Clearly in this scenario, operating the sensor at 10-μA driving current is more favorable in terms of sensor response resolution as it produces a larger response magnitude.

The baseline dc signal variation of a PEVA coated sensor is shown in Fig. 13(a). Prior to odor delivery, the baseline dc variation is 800 mV. The output of the sensor interface circuit after baseline cancellation and a fixed (inverting) amplification is shown in Fig. 13(b). It is seen that the interface circuit is able to compensate the baseline variations thereby facilitating full measurement range amplification to be carried out at the subsequent programmable gain amplifier stage. The slight variation in sensor response is attributed to the lower resolution when the direct sensor responses are measured. The ± 1 bit error of the baseline compensation circuit is found to be ± 5 mV. The typical setup time for baseline cancellation is 512 μs based on a 2-MHz clock. The programmable gain amplifiers implemented on chip have selectable gains of 10, 100, and 1000. The output of the programmable amplifier is filtered using a low-pass OTA-C filter.

E. Measured Neuromorphic Circuits Results

The chip measurements of the neuromorphic circuits are presented in this section. A synapse circuit is tested by exciting it with a spike input with 1 ms duration. The response for the synapse programmed with a weight input of -0.5 V and time constant of 75 ms is shown in Fig. 14(a). Since the sign of the weight is negative with respect to the baseline, the synapse exhibits an inhibitory response. The chip measurements show a

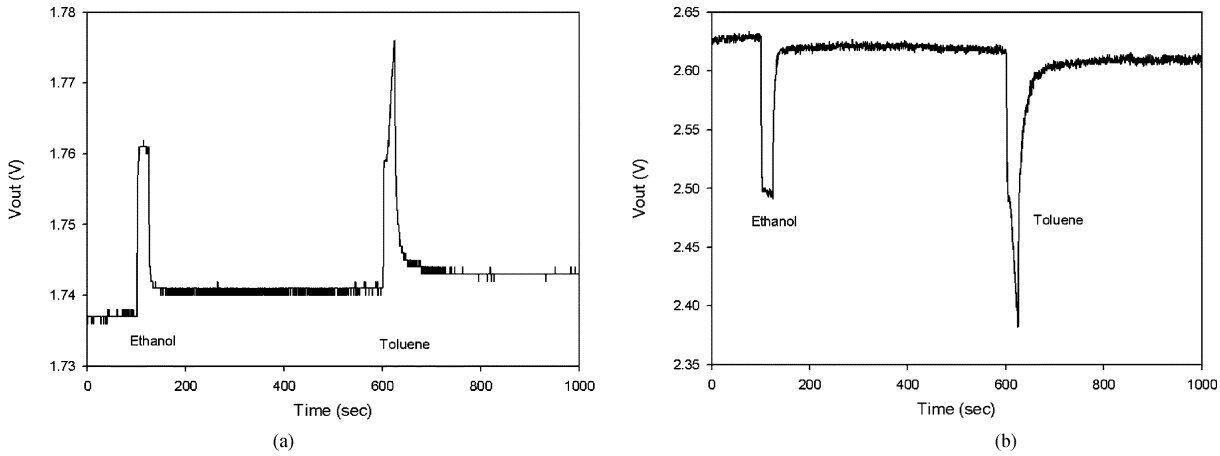

Fig. 13. Sensor responses to ethanol and toluene vapor. (a) Sensor response coated with PEVA on direct measurement. (b) Response of PEVA coated sensor with signal conditioning circuit.

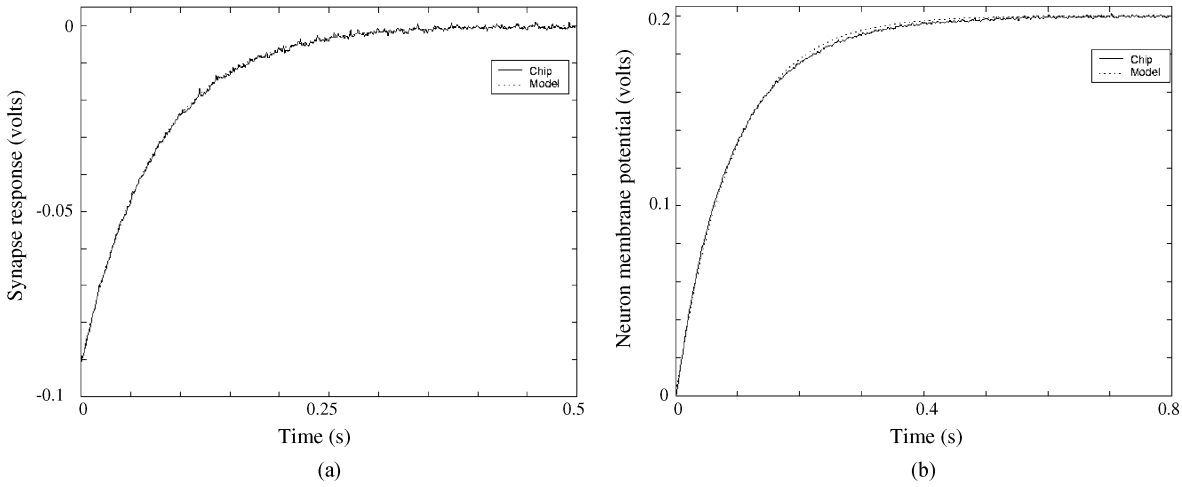

Fig. 14. Chip measurements of synapse response and neuron membrane potential compared to their respective mathematical models: (a) Inhibitory synaptic response $i_{\rm syn}$ (Fig. 5) measured from the chip for a negative weight and a single spike input compared to the mathematical model ((3)). The trailing edge of the spike occurs at time 0 s. $V_{\rm wt} = -0.5$ V and synapse time constant is 75 ms. (b) Membrane potential measured at $C_{\rm int}$ (Fig. 7) compared to mathematical model ((1)). Input is a step of 0.2 V. Membrane time constant is 92 ms.

close match with the mathematical model [see Fig. 14(a)]. Chip measurements of neuron membrane potential response measured at the integrating capacitor $C_{\rm int}$ are shown in Fig. 14(b). The input to the leaky integrator is a step of 0.2 V and membrane time constant is 92 ms. The response shows a close match with the mathematical model of (1) [see Fig. 14(b)].

The functionality of the on-chip learning neuromorphic circuit is independently tested. The output response of the on-chip STDP circuit under two different presynaptic and postsynaptic input spike conditions are shown in Fig. 15. Fig. 15(a) shows the learning response of the synapse when excited by a presynaptic spike preceding the occurrence of a postsynaptic spike by 5 ms. Initially, the synaptic weight is negative causing the synapse to generate an inhibitory response. As the presynaptic spikes arrive prior to the occurrence of postsynaptic spikes, the weight is strengthened and the synaptic response becomes excitatory as shown in Fig. 15(a). Fig. 15(b) shows the synaptic response and weight dynamics when presynaptic spikes follow the occurrence of postsynaptic spikes by 5 ms. Here, the synapse response do not contribute to the firing of the postsynaptic neuron. Hence, the weight is weakened and the synapse response becomes inhibitory. The weight increment (decrement) is smaller if the presynaptic spike precedes (follows) the postsynaptic spike by a larger time interval.

Fig. 16 shows the chip measurements when a receptor neuron is connected to PN through a synapse. A step input of 0.2 V evokes receptor neuron firings at a rate of approximately 25 ms. The repeated receptor neuron firing and synapsing on to the PN eventually causes the PN to fire (see Fig. 16). The summation of exponentially decaying synaptic currents for multiple receptor neuron spike events is also shown in Fig. 16. Importantly, this test result demonstrates the functional signal path through the entire neuromorphic circuit. The measured performance of the neuromorphic olfaction chip components are summarized in Table II.

V. System Circuit Simulation

In this section, analog circuit simulation results of the olfactory neuromorphic network for a simple odor classification experiment are presented. Ethanol and toluene data profiles

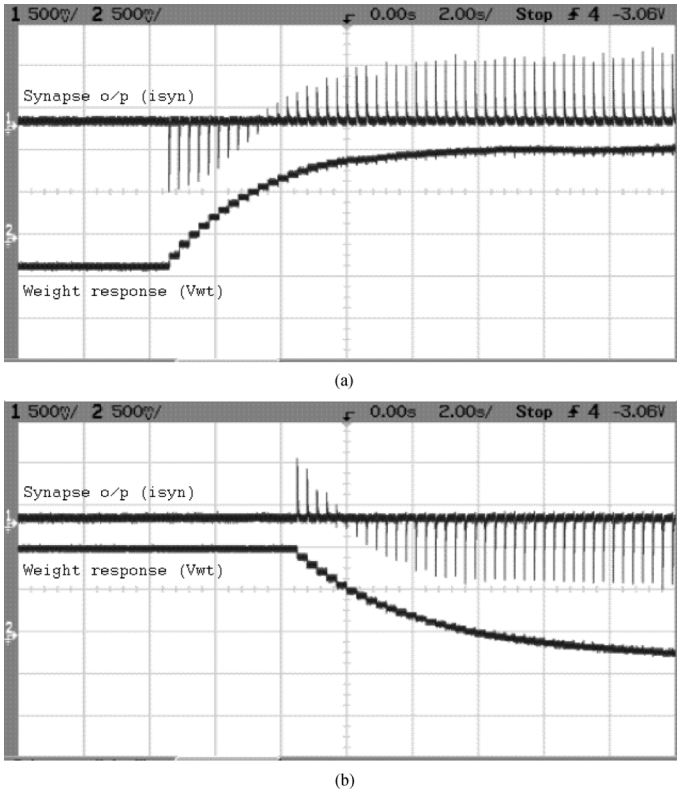

Fig. 15. Chip measurements of weight response $V_{\rm wt}$ and synaptic response $i_{\rm syn}$ during on-chip STDP learning. The circuit is driven by a series of pre and postsynaptic spike pairs where (a) the presynaptic spike occurs 5 ms before the postsynaptic spike and (b) the presynaptic spike occurs 5 ms after the postsynaptic spike. The weight responses $V_{\rm wt}$ show weight strengthening in (a) and weight weakening in (b).

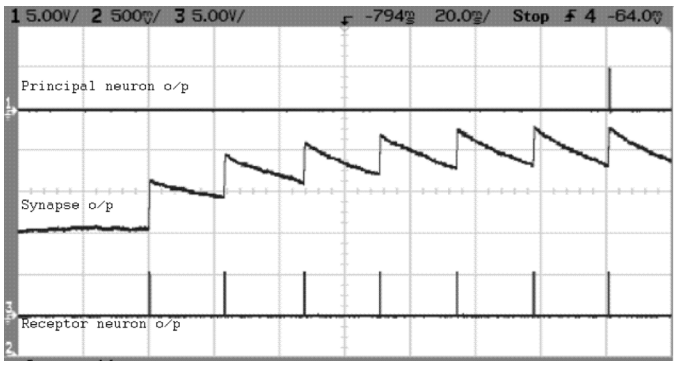

Fig. 16. Chip measurements showing the receptor neuron firing and synapsing on to the PN eventually causing it to fire. This result demonstrates the functional signal path through the entire neuromorphic circuit. Summation of exponentially decaying synaptic currents $i_{\rm syn}$ for multiple receptor neuron spike events is also shown.

measured from our chemosensor array are used in this study (Fig. 11). The experimental setup for sensor measurement is discussed in Section IV-C. Here the olfactory neuromorphic architecture shown in Fig. 2 has been used. The network receives input signals from 6 sensors and has two outputs (PN1 and PN2). PEVA, and PSB sensor types are used as the input chemosensors for the neuromorphic network. In the network architecture of Fig. 2 sensors 1 – 3 are PEVA type and sensors 4 – 6 are PSB type. The amplitudes of similar sensor types are

TABLE II
MEASURED PERFORMANCE SUMMARY OF THE ADAPTIVE NEUROMORPHIC OLFACTION CHIP

Parameter	Values
Technology	0.6 μm
Supply voltage	5 V
Area	6.5 mm^2
Sensor resistance	10 KΩ - 200 KΩ
Sensor driving current	1 μA, 10 μA, 100 μA
Sensor bandwidth	$<$ 1 Hz
Sensor DC baseline variation	$\pm$1 V
Input referred DC offset	$<\pm$5 mV
Prog. amplifier gains	10, 100, 1000
Synaptic time constant	10ms - 300 ms
Weight range	$\pm$1 V
Neuron time constant	10 ms - 300 ms
Neuron spike width	10 μs - 1 ms
Neuron refractory time period	10 ms - 300 ms

normalized to account for the varying sensitivity observed at different locations in the array, while the profiles are delayed ± 20 ms around the measured data to model retention effects of analyte vapors as they travel along a microchannel. As the measured sensor data is noisy, no additional noise is added to the signals. However, two additional receptor neurons (RN7 and RN8) are added to the network to study noise rejection properties. RN7 and RN8 are connected through feedforward synapses to PN1 and PN2 respectively. All RNs have a time constant of 200 ms. The threshold voltages of all the RN's are set at 70% of the peak sensor signal amplitude. To initiate learning in the network, the threshold voltages of PNs are chosen such that they spike on the arrival of first few correlated RN spikes. The refractory period of the RNs and the PNs are 60 and 120 ms, respectively. The STDP window function is set at ± 50 ms. The circuits of the individual building blocks used in this network simulation have been validated against measured chip results.

A. Network Response

The firing patterns of the neuromorphic network for ethanol input vapor are shown in Fig. 17. Here, RN1-RN3, corresponding to PEVA sensors, produce spikes while the outputs of RN4-RN6 corresponding to PSB sensors do not fire. This is because the PSB sensor signals are too small to cause RN4-RN6 to fire. The RN1-RN3 spikes induce firing in PN1.

The response of the neuromorphic network to toluene input vapor is shown in Fig. 18. Here RN1-RN3, corresponding to PEVA sensors, start firing earlier than RN4-RN6. This correlated response contributes to firing of PN1, thereby strengthening the weights of synapses connecting RN1-RN3 to PN1 as shown in Fig. 19. PN1 firing generates an inhibitory response at the lateral synapse connecting PN1 to PN2 thereby delaying the firing of PN2. However, when RN4-RN6 start firing the synaptic current to PN2 is increased causing PN2 to fire. As PN2 fires, the weights connected to the contributing synapses of PSB receptor neurons (RN4-RN6) get strengthened as shown in Fig. 19.

B. Interpretation of Results

In this system, odor discrimination is provided by both the chemosensors and the neuromorphic system. In the case of

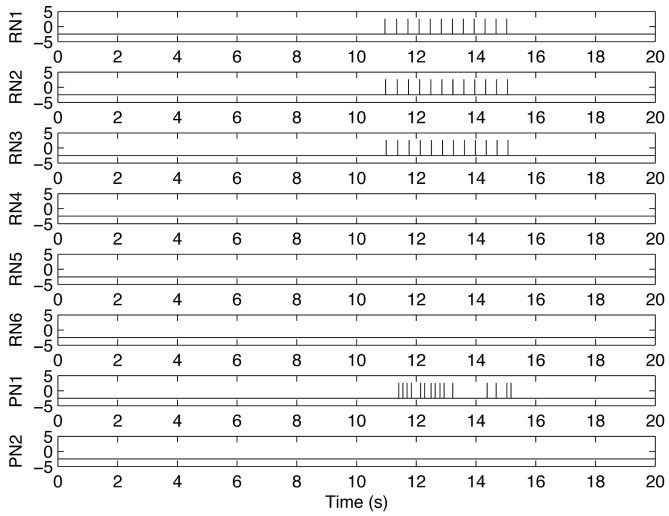

Fig. 17. Neuromorphic network circuit simulation (Cadence Spectre) showing the firing response of RN1-RN6 and PN1-PN2 to the ethanol input odor of Fig. 11(a). Y axis is in volts. The circuits use ± 2.5 V supply voltage. The vertical lines indicate neuronal spikes. RN1-RN3 are excited by PEVA type sensors, RN4-RN6 are excited by PSB type sensors. Sensors respond to odor stimulus at 10 s [see Fig. 11(a)]. The RN1-RN3 spikes induce firing in PN1. There is no spiking activity in PN2.

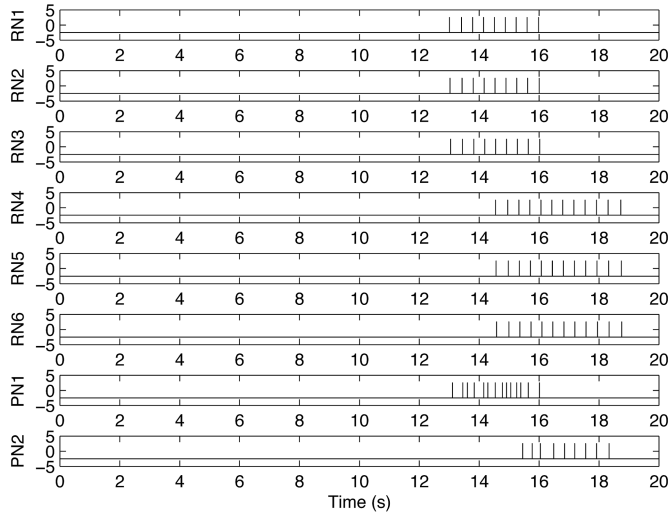

Fig. 18. Neuromorphic network circuit simulation showing the firing response of RN1-RN6 and PN1-PN2 to the toluene input odor of Fig. 11(b). Sensors respond to odor stimulus at 10 s. Y axis is in volts. RN1-RN3 are excited by PEVA type sensors, RN4-RN6 are excited by PSB-type sensors.

ethanol vapor [Fig. 11(a)], the amplitude difference between the two sensor responses provides sufficient discrimination information to allow the neuromorphic system to implement a simple thresholding function at the RN stage to separate the two classes. STDP learning strengthens the weights connecting corresponding sensors to RN1-RN3 to further enhance odor selectivity (weights not shown).

In the case of toluene vapor [Fig. 11(b)], both sensor types have similar amplitude levels and hence a simple thresholding scheme based upon this aspect of the data is not sufficient. Discrimination information from the sensory stage is provided by the transient or temporal response of the sensors to the odor

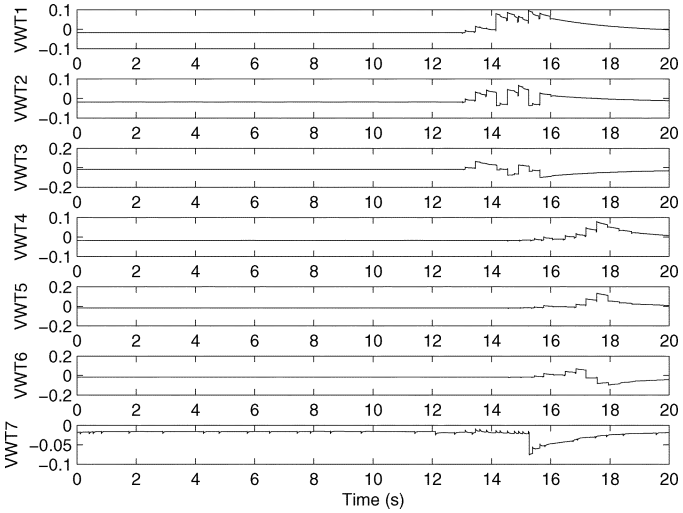

Fig. 19. Neuromorphic network circuit simulation showing the evolution of weights during STDP learning of the toluene input odor. The Y axis is in volts. VWT1-VWT7 are the weight voltages of synapses connected to RN1-RN7. RN7 is excited by a noise source and its weight is weakened during learning.

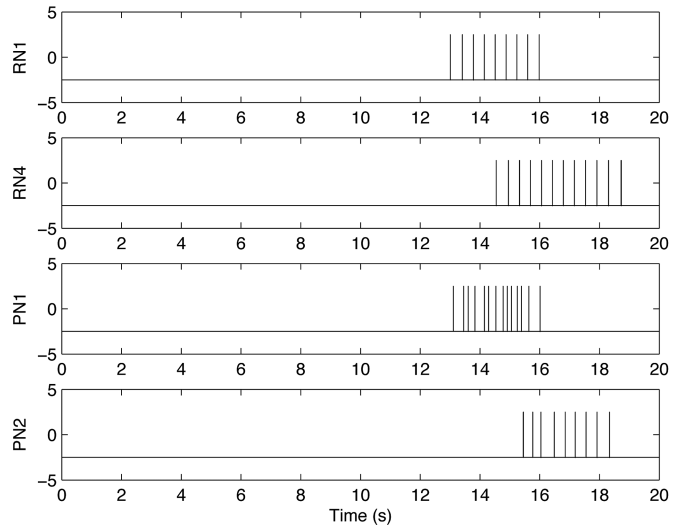

Fig. 20. Network circuit simulation for the toluene input odor [see Fig. 11(b)] showing time delay amplification at the neuromorphic stage. The delay between RN1 and RN4 (1.5 s) first firing is amplified in the response of PN1 and PN2 (2.3 s).

signal and the neuromorphic stage has to extract this transient sensor information to enhance the discrimination of the input odors. The time difference between RN1-RN3 first firing and RN4-RN6 first firing was 1.5 s. The same measurement difference between PN1 and PN2 first firings was 2.3 s (see Fig. 20). The role of the neuromorphic system here could be interpreted as an amplification of this time delay thereby improving the separation between these two odor signals.

Spikes from RN7 and RN8 are driven by random noise sources. Here, STDP learning scheme weakens the weights connected to RN7 and RN8 as they arrive out of synchrony with the sensor signals (see Fig. 19 for adaption of weight $V_{\mathrm{wt}7}$ connected to RN7). This improves the noise performance of the system.

These simulations are obtained using simple odor samples measured from test experiments conducted on our olfaction sensor chip. These simulations are neither an exhaustive nor a comprehensive study of the problem of identifying odors in complex backgrounds.

VI. Conclusion and Future Work

In this paper, we have presented the analog VLSI implementation of the circuit building blocks of an adaptive neuromorphic olfaction chip developed over a number of chip implementation cycles. During the course of the work several circuit design challenges were addressed. On the sensory front, the main circuit design challenge was to compensate the large variation in sensor baseline signals in the chemosensor array leading to loss of measurement range which cannot be recovered. A dc cancellation circuit was implemented on chip to cancel the baseline sensor variations. In the neuromorphic implementation, the key challenge was to design circuits with large time constants while keeping the neuronal structure simple and occupying small silicon area. The neuron, synapse and on-chip learning circuits were all implemented using simple OTA-C structures. Time constants in the range of 300 ms were achieved by reducing the transconductance of the OTA stage thereby alleviating the need to implement large area capacitors.

Our vision is to build a fully integrated neuromorphic olfactory device in analog VLSI. To attain this goal, we have demonstrated that all the subsystem components are successfully working in silicon. Moreover, by fabricating and testing two separate chips with a sensor array and a neuromorphic array, we have attained significant understanding of the working of these analog circuit blocks when connected together in large arrays. A further prototype chip with an on-chip chemosensor array, on-chip sensor interface circuitry and on-chip adaptive neuromorphic circuitry has been fabricated using AMS 0.6-μm CMOS technology. The architecture of the chip implements a slice of an olfactory pathway such that a scalable olfactory network can be constructed by interconnecting multiple chips. Our next step is to test and evaluate the performance of this system when subjected to input odors.

A number of challenges are anticipated in the final integration of a complete system. Careful deposition of the sensing materials with a broad diversity of chemical sensitivity will be required together with a screening process for each sensor to ensure the output chemical response is ideal for odor recognition. Circuits and systems issues such as long term weight storage, component mismatch, layout optimization, decoding of spike outputs or the use of an address event representation (AER) [42] interface for instance should be considered.

References

[1] R. L. Doty, *Handbook of Olfaction and Gustation*, 2nd ed. New York: Marcel Dekker, 2003.

[2] T. C. Pearce, S. S. Schiffman, H. T. Nagle, and J. W. Gardner, *Handbook of Machine Olfaction*. New York: Wiley-VCH, 2003.

[3] J. W. Gardner and P. N. Barlett, *Electronic Noses–Principles and Applications*. New York: Oxford University Press, 1999.

[4] T. A. Dickinson, J. White, J. S. Kauer, and D. R. Walt, "Current trends in "artificial-nose" technology," *Trends Biotechnol.*, vol. 16, no. 6, pp. 250–258, 1998.

[5] K. Mori, H. Nagao, and Y. Yoshihara, "The olfactory bulb: Coding and processing of odor molecule information," *Science*, vol. 286, p. 711, 1999.

[6] J. A. Covington, S. L. Tan, J. W. Gardner, A. Hamilton, T. J. Koickal, and T. C. Pearce, "Combined smart chemFET/resistive sensor array," in *Proc. IEEE Sensor Conf.*, 2003, vol. 2, pp. 22–24.

[7] A. G. Lozowski, M. Lysetskil, and J. M. Zurada, "Signal processing with temporal sequences in olfactory systems," *IEEE Trans. Neur. Networks*, vol. 15, no. 5, pp. 1268–1275, Sep. 2004.

[8] N. Caticha, J. E. P. Tejada, D. Lancet, and E. Domany, "Computational capacity of an odorant discriminator: The linear separability of curves," *Neur. Computation*, vol. 14, pp. 2201–2220, 2002.

[9] B. Raman, P. A. Sun, A. Gutierrez-Galvez, and R. Gutierrez-Osuna, "Processing of chemical sensor arrays with a biologically inspired model of olfactory coding," *IEEE Trans. Neur. Networks*, vol. 17, no. 4, pp. 1015–1024, Jul. 2006.

[10] C. D. Brody and J. J. Hopfield, "Simple networks for spike-timing-based computation, with application to olfactory processing," *Neuron*, vol. 37, no. 5, pp. 843–52, 2003.

[11] J. J. Hopfield, "Odor space and olfactory processing: Collective algorithms and neural implementation," *Proc. Natl. Acad. Sci. USA*, vol. 96, no. 22, pp. 12506–12511, 1999.

[12] T. A. Dickinson, J. White, J. S. Kauer, and D. R. Walt, "An olfactory neuronal network for vapor recognition in an artificial nose," *Biol. Cybernetics*, vol. 382, pp. 697–700, 1996.

[13] M. Pardo and G. Sberveglieri, "Remarks on the use of multilayer perceptrons for the analysis of chemical sensor array data," *IEEE Sensors J.*, vol. 4, pp. 355–363, Jun. 2004.

[14] P. Boilot, E. L. Hines, J. W. Gardner, R. Pitt, S. John, J. Mitchell, and D. W. Morgan, "Classification of bacteria responsible for ENT and eye infections using the cyranose system," *IEEE Sensors J.*, vol. 2, pp. 247–253, 2002.

[15] J. Perez-Orive, O. Mazor, G. C. Turner, S. Cassenaer, R. I. Wilson, and G. Laurent, "Oscillations and sparsening of odor representations in the mushroom body," *Science*, vol. 297, pp. 359–365, 2002.

[16] L. I. Zhang, H. W. Tao, C. E. Holt, W. A. Harris, and M. M. Poo, "A critical window for cooperation and competition among developing retinotectal synapses," *Nature*, vol. 395, pp. 37–44, 1998.

[17] W. Gerstner, R. Kemter, J. L. van Hemmen, and H. Wagner, "A neuronal rule for sub-millisecond temporal coding," *Nature*, vol. 383, pp. 76–78, 1996.

[18] S. Song, K. D. Miller, and L. F. Abbott, "Competitive Hebbian learning through spike-timing-dependent-plasticity," *Nature Neuroscience*, vol. 3, no. 9, pp. 919–926, 2000.

[19] S. M. Bohte, "The evidence for neural information processing with precise spike-times: A survey," *Natural Computing*, vol. 3, pp. 195–206, 2004.

[20] H. Markram, J. Lubke, M. Frotscher, and B. Sakmann, "Regulation of synaptic efficacy by coincidence of postsynaptic APs and EPSPs," *Science*, vol. 275, pp. 213–215, 1997.

[21] G.-Q. Bi and M. M. Poo, "Synaptic modifications in cultured hippocampal neurons; dependence on spike timing, synaptic strength and postsynaptic cell type," *J. Neurosci.*, vol. 18, pp. 10464–10472, 1998.

[22] G.-Q. Bi and H.-X. Wang, "Temporal asymmetry in spike timing-dependent plasticity," *Physiol. Behavior*, vol. 77, pp. 551–555, 2002.

[23] A. P. Shon, R. P. N. Rao, and T. J. Sejnowski, "Motion detection and prediction through spike-timing dependent plasticity," *Network: Comput. Neur. Syst.*, vol. 15, no. 3, pp. 179–198, 2004.

[24] P. Mombaerts, F. Wang, C. Dulac, S. K. Chao, A. Nemes, M. Mendelsohn, J. Edmondson, and R. Axel, "Visualizing an olfactory sensory map," *Cell*, vol. 87, no. 14, pp. 675–686, 1996.

[25] J. I. Egana, M. L. Aylwin, and P. E. Maldonado, "Odor response properties of neighboring mitral/tufted cells in the rat olfactory bulb," *Neuroscience*, vol. 134, no. 3, pp. 1069–80, 2005.

[26] T. C. Pearce, C. Fulvi-Mari, J. A. Covington, F. S. Tan, J. W. Gardner, T. J. Koickal, and A. Hamilton, "Silicon-based neuromorphic implementation of the olfactory pathway," in *Proc. IEEE EMBS Conf. Neural Eng.*, 2005, pp. 307–312.

[27] E. J. Severin, B. J. Doleman, and N. S. Lewis, "An investigation of the concentration dependence and response to analyte mixtures of carbon black/insulating organic polymer composite vapor detectors," *Anal. Chem.*, vol. 72, pp. 658–668, 2000.

[28] J. A. Dickson, M. S. Freund, N. S. Lewis, and R. M. Goodman, "An integrated chemical sensor array using carbon black polymers and a standard CMOS process," in *Tech. Dig.Solid-State Sensor and Actuator Workshop*, 2000, pp. 162–165.

[29] R. W. Cattral, *Chemical Sensors*. Oxford, U.K.: Oxford Univ. Press, 1997.
[30] S. Y. C. Catunda, J.-F. Naviner, G. S. Deep, and R. C. S. Freire, "Designing a programmable analog signal conditioning circuit without loss of measurement range," *IEEE Trans. Instrum. Measur.*, vol. 52, no. 5, pp. 1482–1487, Oct. 2003.
[31] T. J. Koickal, A. Hamilton, S. L. Tan, J. A. Covington, J. W. Gardner, and T. C. Pearce, "Smart interface circuit to ameliorate loss of measurement range in chemical microsensor arrays," in *Proc. IEEE Instrum. Measur. Conf.*, 2005, vol. 1, pp. 548–550.
[32] M. Steyaert, P. Kinget, and W. Sansen, "Full integration of extremely large time constants in CMOS," *Electron. Lett.*, vol. 27, no. 10, pp. 790–791, 1991.
[33] C. Mead, *Analog VLSI and Neural Systems*. Reading, MA: Addison-Wesley, 1989.
[34] J. P. Lazzaro and J. Wawrzynek, "Low-power silicon axons, neurons, and synapses," in *Silicon Implementations of Pulse Coded Neural Networks*, M. E. Zaghloul, J. L. Meador, and R. W. Newcomb, Eds. Norwell, MA: Kluwer Academic Publishers, 1994, pp. 153–164.
[35] K. A. Boahen, "The retinomorphic approach: Pixel-parallel adaptive amplification, filtering, and quantization," in *Neuromorphic Systems Engineering*, T. S. Lande, Ed. Boston, MA: Kluwer , 1998, pp. 229–261.
[36] C. Rasche and R. H. R. Hahnloser, "Silicon synaptic depression," *Biol. Cybern.*, vol. 84, pp. 57–62, 2001.
[37] M. Boegerhausen, P. Suter, and S. Liu, "Modeling short-term synaptic depression in silicon," *Neur. Comput.*, vol. 15, no. 2, pp. 331–348, 2003.
[38] J. V. Arthur and K. Boahen, "Recurrently connected silicon neurons with active dendrites for one-shot learning," in *Proc. Int. Conf. Neur. Networks*, 2004, pp. 1699–1704.
[39] R. Z. Shi and T. Horiuchi, "A summating exponentially decaying CMOS synapse for spiking neural systems," in *Advances in Neural Information Processing Systems*, S. Thrun, L. Saul, and B. Scho''lkopf, Eds. Cambridge, MA: MIT Press, 2004, vol. 16, pp. 1033–1010.
[40] G. Indiveri, E. Chicca, and R. Douglas, "A VLSI array of low-power spiking neurons and bistable synapses with spike-timing dependent plasticity," *IEEE Trans. Neur. Networks*, vol. 17, no. 1, pp. 211–221, Jan. 2006.
[41] A. Bofill-i-Petit and A. F. Murray, "Synchrony detection and amplification by silicon neurons with STDP synapses," *IEEE Trans. Neural Networks*, vol. 15, no. 5, pp. 1296–1304, Sep. 2004.
[42] K. A. Boahen, "Point-to-point connectivity between neuromorphic chips using address-events," *IEEE Trans. Circuits Syst. II, Analog Digit. Signal Process.*, vol. 47, no. 5, pp. 416–434, May 2000.

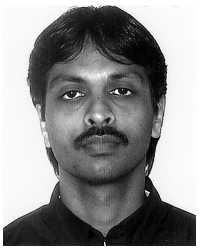

Thomas Jacob Koickal received the Ph.D degree in electronics and electrical communication engineering from Indian Institute of Technology, Kharagpur, India.

From 1998 to 2002, he was a Scientist in the Control and Guidance Design Group at Vikram Sarabhai Space Center, Trivandrum, India. Since 2002, he has been a Research Fellow in the School of Engineering and Electronics, University of Edinburgh, Edinburgh, U.K. His current research interests include biologically inspired circuit designs, time event based computing and programmable analog VLSI architectures.

Alister Hamilton is a Senior Lecturer in the discipline of electronics in the School of Engineering and Electronics at the University of Edinburgh, Edinburgh, U.K., were he has worked since 1988. His research interests are in the implementation of neural networks and neuromorphic systems in analog VLSI and in novel design strategies for programmable analog arrays.

Su Lim Tan (M'06) received the Ba.Sc. degree in computer engineering infrom Nanyang Technological University, Singapore, in 1999, and the Ph.D. degree in electronic engineering from the University of Warwick, Warwick, U.K., in 2005.

He is currently a lecturer at the School of Computer Engineering, Nanyang Technological University. His research interests include embedded systems design, wireless sensor networking, machine olfaction and biomedical instrumentation.

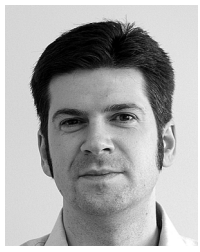

James A. Covington received the B.Eng. degree in electronic engineering and the Ph.D. degree from the University of Warwick, Warwick, U.K., in 1996 and 2000, respectively. His doctoral work focused on the development of CMOS and systems-on-insulator CMOS gas sensors for room temperature and high temperature operation.

He is presently an Associate Professor in the School of Engineering at the University of Warwick. He was a Research Fellow for both the University of Warwick, and and Cambridge University, working on the development of gas and chemical sensors and was appointment as a Lecturer at the University of Warwick in 2002. His current research interests focuses on the development of silicon devices with novel materials using CMOS and systems-on-insulator application-specific integrated circuit technology (nose-on-a-chip), and biologically inspired neuromorphic devices with applications based on environmental and biomedical engineering.

Julian W. Gardner (SM'02) is Professor of Electronic Engineering in the School of Engineering at the University of Warwick, Warwick, U.K. He is also Dean of Engineering at the University of Warwick. His research interests include the modeling of silicon microsensors, chemical sensor array devices, biomimetic microelectromechanical devices, and electronic noses. He has worked with over 20 companies in the past 15 years developing commercial e-nose instruments and a Consultant for various companies. He is author or coauthor of over 350 technical papers and patents as well as six technical books in the area of microsensors and machine olfaction.

Dr. Gardner is Series Editor for a books series by Wiley-VCH. He is a Fellow of the IEE and senior member of the IEEE and serves on several advisory panels on sensors, e.g., for EPSRC, DTI, and IEE Professional Network on Microsystems and Nanotechnology. He is a Fellow of the Royal Academy of Engineering.

Tim C. Pearce Photograph and biography not available at the time of publication.